ACS APPLIED MATERIALS & INTERFACES

Research Article

www.acsami.org

Li Intercalation into a β-MnO_2 Grain Boundary

James A. Dawson* and Isao Tanaka

Department of Materials Science and Engineering, Kyoto University, Sakyo, Kyoto 606-8501, Japan

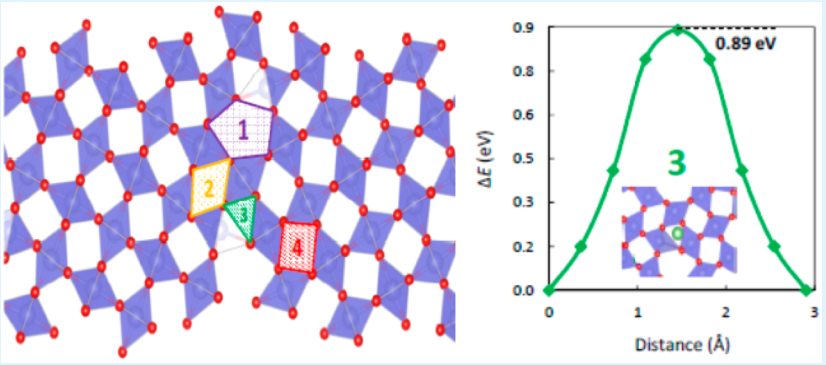

ABSTRACT: MnO_2 is well-known for its technological applications including Li ion, Li−air batteries, and electrochemical capacitors. Compared to the bulk material, nanostructuring of rutile (β-)MnO_2 has been shown to vastly improve its electrochemical properties and performance. While the bulk material cannot readily intercalate Li, nanostructured mesoporous samples exhibit good Li intercalation. This observation is not yet fully understood. In this work, we use state-of-the-art theoretical techniques to investigate Li intercalation and migration at the β-MnO_2 Σ 5(210)/[001] grain boundary (GB). We show how large tunnel structures in the GB can promote Li intercalation with voltages of up to 3.83 eV compared to the experimental value of 3.00 eV. Conversely, small tunnel structures resulting from overcoordination of ions at the GB can hinder Li intercalation with significantly reduced voltages. The size and shape of these tunnels also strongly influence the energetics of Li migration with energy barriers ranging from 0.15 to 0.89 eV, compared to a value for the bulk of 0.17 eV. Our results illustrate how GBs with large, open tunnel structures may promote electrochemical performance and could be a contributing factor to the excellent performance of nanostructured β-MnO_2.

KEYWORDS: *cathode material, grain boundaries, catalyst, lithium battery, supercapacitor*

1. INTRODUCTION

The search for materials with higher energy capacity and storage for various applications including hybrid electric vehicles and renewable energy sources is one of the most popular and important topics in materials and energy science. Many conventional battery and catalytic materials have significant disadvantages, for example, the cost of $LiCoO_2$ and the difficulty in its disposal. Whereas β-MnO_2 as an electrode material and catalyst is easy to prepare, low in cost, and low in toxicity.[1] In recent years, the search for safer, cheaper, and more efficient energy storage materials has resulted in considerable research of bulk manganese oxides[1−3] as well as their surfaces[4−6] and grain boundaries (GBs).[7,8]

Studies of bulk β-MnO_2 show no significant Li-ion intercalation,[9,10] whereas nanocompsite and mesoporous β-MnO_2 is used as a cathode material for Li ion batteries as it exhibits good Li-ion intercalation,[11,12] high capacities[9,11,13] of up to 320 $mAhg^{-1}$, and good cycling stability.[9] Increased Li diffusion in nanosized materials has also been confirmed by ac impedance measurements.[14] Another important application of MnO_2 is as a catalyst for a variety of reactions. One example is in electrochemical ORRs, which are essential in a variety of energy storage and conversion applications including metal−air batteries and fuel cells.[6,15,16] This technology is also fundamental to the Li−O_2 battery system, which is an alternative to conventional Li-ion batteries and could potentially significantly increase specific energy density.[17] A summary of other catalytic applications of manganese oxides is available elsewhere.[4] In addition to battery and catalytic applications, nanostructured β-MnO_2 also shows potential as a supercapacitor electrode material.[18,19] Upon nanostructuring of the material, a significant increase in the capacitance (285 Fg^{1-})[18,19] is observed when compared to the bulk material.

Despite the fact that the increased surface area resulting from nanostructuring is essential in significantly improving the electrochemical properties of β-MnO_2, a complete understanding of why this happens is still lacking. However, in recent years there have been several works that have attempted to further clarify the role of interfaces in this material. Tompsett et al.[5] used density functional theory (DFT) with the generalized gradient approximation (GGA) and Hubbard U corrections to consider the importance of surface to bulk Li-ion migration in

Received: January 29, 2015
Accepted: March 26, 2015
Published: March 26, 2015

DOI: 10.1021/acsami.5b00775
ACS Appl. Mater. Interfaces 2015, 7, 8125−8131

β-MnO_2. They calculated a low value of 0.17 eV for Li migration in the bulk but obtained a far larger value of >0.6 eV for Li insertion at the (101) surface (the dominant surface in equilibrium morphology). These results clearly illustrate the difficulty of intercalating Li into bulk samples of β-MnO_2. Mellan et al.[20] used the same computational approach for calculating lithium and oxygen adsorption at the (110) surface of β-MnO_2 for its application in Li−air batteries. Various other studies, for a range of applications, on the surfaces of β-MnO_2 are available in the literature.[4,6,21−23]

With regard to β-MnO_2 GBs, two theoretical studies have been completed, both with the focus on oxygen vacancy formation for catalytic applications. In the first study,[7] interatomic potential methods were used to investigate the lowest energy structures for a number of β-MnO_2 grain boundaries (GBs) and to calculate the energies of Mn^{4+} reduction and oxygen vacancy formation. Both reduction and oxygen formation energies were shown to be favored in and around the GB core, suggesting a potentially higher catalytic activity at the GBs. The second study[8] used GGA+U calculations to also show low energy oxygen vacancy formation at the Σ 5(210)/[001] GB, and in some cases the formation energies calculated were even lower than those calculated for β-MnO_2 surfaces.[4] Oxygen vacancy formation at the GB was also shown to produce metallic behavior which could be responsible for the creation of conductive GB pathways. GBs play a significant role in determining the properties of bulk materials, however, there is still debate over the GB concentration in the more electrochemically active nanostructured samples. While some believe it is easy to anneal GBs and dislocations out of the samples because of the close vicinity of internal surfaces, others believe that the concentration of GBs is higher in nanostructured materials because of fabrication using self-assembly of nanobuilding blocks and/or nanocasting. Furthermore, as grain sizes are reduced in nanostructured samples, the GB volume is effectively increased. It is also highly likely that GBs adjacent to the active surfaces in these samples are also important in influencing the electrochemical properties. It is therefore essential that studies focusing on GBs are completed for comparison with previous surface and bulk studies.

Building upon our previous study,[8] in this work, we use GGA+U calculations to analyze Li intercalation and migration at the β-MnO_2 Σ 5(210)/[001] GB. We begin by describing our computational approach and justifications for using such methods. This is followed by details of the GB local structure with particular attention given to the size and shape of the tunnels which act as Li migration pathways. We then discuss the results for the calculations of Li intercalation voltage. Finally, we focus on Li migration through the tunnel structures of the β-MnO_2 Σ 5(210)/[001] GB.

2. METHODOLOGY

All calculations were completed using DFT+U calculations with the GGA[24] and projector augmented-wave (PAW)[25] methods as implemented in the VASP[26] code. We use a cutoff energy of 500 eV for all calculations. A k-point grid of 3 × 2 × 2 was used for the GB supercell calculations. The value of the U parameter used for our calculations was chosen on the basis of our previous work[8] and other previous works on β-MnO_2 surfaces.[3,4] The values were determined using Wien2k[27,28] and have been shown to accurately describe Li intercalation, band gaps, and magnetic interactions.[4] However, it is only when the U parameter is applied in the fully localized limit that such descriptions are achieved. Further details on the impact of the values and nature of the U parameter on this material are available in a previous publication.[29] The fully localized limit is used in this work, and we employ values of $U - J$ = 5.1 eV, for the spherical part of the interaction, and J = 1.0 eV. A collinear antiferromagnetic ordering is used in all our calculations. More details on the magnetic structures of this material and the differences in simulating them are available elsewhere.[8,29]

The Σ 5(210)/[001] GB was chosen for this work on the basis of our two previous β-MnO_2 GB studies.[7,8] Lattice statics calculations[7] found that the Σ 5(210)/[001] GB was the lowest energy out of a number of GBs tested. GGA+U calculations[8] confirmed this and produced a very stable GB energy of 0.36 Jm^{-2}. This GB structure has also been confirmed as an important microtwinning plane in ramsdellite MnO_2.[30−33] Microtwinning has also been confirmed in β-MnO_2[13,30−33] and has been shown to be crucial in helping the insertion of Li ions into the internal surfaces of nanoporous MnO_2.[13,33] This GB is also commonly observed in rutile structures and has been featured in numerous studies of TiO_2 GBs.[34−36] Details on the construction of the GB and how the lowest energy structure is found are available in our previous study.[8]

Minimum energy path calculations between two optimized, stable Li sites were completed using the NEB method where the migration path is divided into a number of equidistant configurations known as images. For all the Li migration calculations in this work, seven images are used. Simple linear interpolations between the initial and final Li sites were used for the migration pathways. The images of the migration path are connected with springs and their positions optimized. In the NEB method, optimization uses the spring force along the direction of the migration path (to prevent the images from sinking into the minima) in addition to the true force along the direction perpendicular to the migration path (to ensure the lowest energy path is obtained).

3. RESULTS AND DISCUSSION

3.1. Structures. Bulk β-MnO_2 is tetragonal with space group $P4/mnm$ (136) and has lattice parameters of a = 4.398 Å and c = 2.873 Å.[37] Our GGA+U calculations predict lattice parameters of a = 4.439 Å and c = 2.932 Å; these values are within 2% of the experimental values and illustrate the typical overestimation of GGA calculations. Upon Li intercalation, the tetragonal symmetry reduces to orthorhombic space group $Pnnm$ (58), and Jahn−Teller distortion, arising from the reduction of Mn^{4+} to Mn^{3+}, causes a contraction of the c-axis and an expansion of the other two lattice parameters.[5,38] X-ray diffraction gives lattice parameters for β-$LiMnO_2$ as a = 5.142 Å, b = 5.003 Å, and c = 2.813 Å.[38] Our GGA+U calculations give values of a = 5.221 Å, b = 5.191 Å, and c = 2.861 Å and again show its tendency for overestimation of the unit cell volume. The values are again within 2% of the experimental values. The β-$LiMnO_2$ structure and the three potential Li migration pathways are displayed in Figure 1. Previous computational studies have ruled out the two migration pathways in Figure 1a, as their distances and therefore migration energies are far too large.[1,5] This suggests that Li diffusion in this material is 1D and that it occurs through channels along the c-axis as confirmed by experiment.[39,40] On this basis, we only consider Li diffusion along the c-axis in this study.

For all our GB calculations, we use a supercell of 288 ions with dimensions of a = 5.82 Å, b = 13.96 Å, and c = 33.76 Å. It

DOI: 10.1021/acsami.5b00775
ACS Appl. Mater. Interfaces 2015, 7, 8125−8131

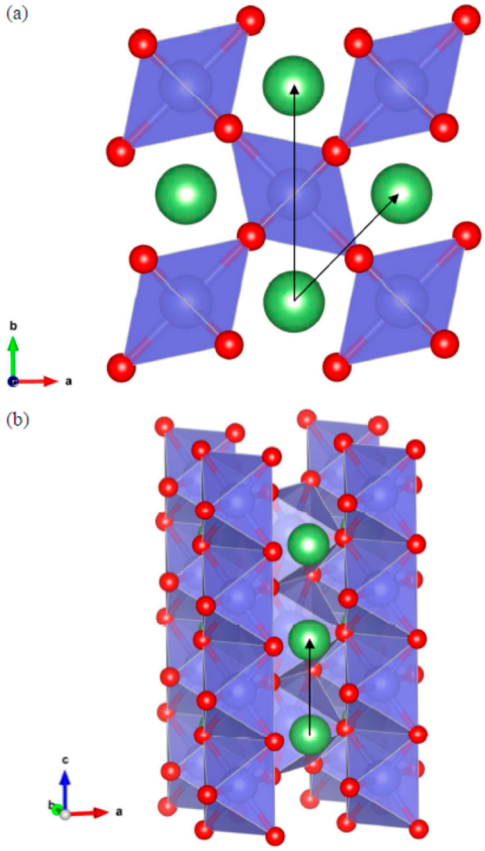

Figure 1. Crystal structure of lithiated β-MnO_2 ($LiMnO_2$) viewed (a) along the *c*-axis and (b) obliquely. Red spheres represent oxygen ions, blue spheres are Mn ions, and green spheres are Li ions. The black arrows illustrate the three possible Li migration paths.

is essential all GB structures are longest in the *z* direction in order to minimize the interactions between the equivalent GBs at the center and edges of the supercells. Figure 2 shows the optimized Σ 5(210)/[001] GB used for the calculations in this work. For further details about the local structure of this GB and its electronic properties, please refer to our previous study.[8] Figure 2 also shows the four tunnel structures considered for Li

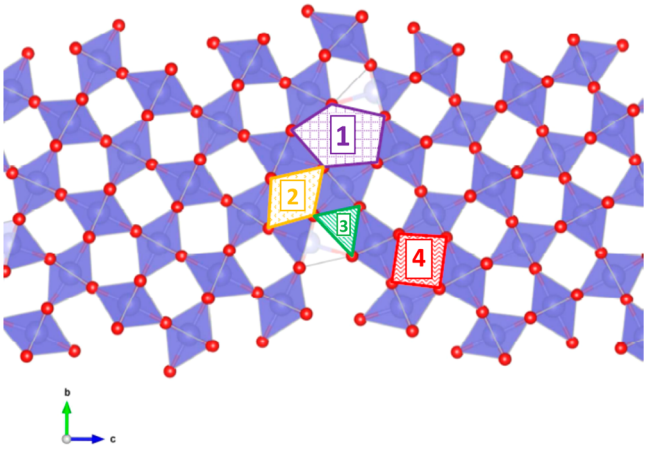

Figure 2. Optimized, lowest energy β-MnO_2 Σ 5(210)/[001] GB configuration illustrating the four tunnel structures considered for Li intercalation and migration. The two clear, transparent octahedra at the GB represent overcoordinated Mn ions.

intercalation and migration are also displayed. These structures vary significantly and therefore give a good representation of the different structural environments present in a GB for the calculation of intercalation and migration properties. Tunnel 1 is by far the largest of the four structures and results from the significant MnO_6 octahedral distortion at the GB. Tunnel 2 is similar to a normal *c*-axis channel in the bulk structure, however, the shape is more elongated. Tunnel 3 is the smallest tunnel and is highly distorted; it again results from the strong distortion at the GB and the overcoordination of some Mn ions. The final tunnel is almost identical to the tunnel structure in the bulk which allows us to test the effect of the adjacent GB on a nonhighly distorted bulk-like channel.

3.2. Intercalation Voltages. The amount of electrical energy that a battery can deliver is a function of the cell potential (V) and capacity ($Ahkg^{-1}$). Therefore, materials with high intercalation energy and as a result, higher voltages, are essential for electrochemical systems. DFT calculations are now commonly used to predict intercalation voltages for a vast range of materials.[41,42] The intercalation energy is calculated by

$$E_{int} = \frac{E_{MnO_2/nLi} - (E_{MnO_2} + nE_{Li})}{n\text{Li}} \quad (1)$$

where E_{int} is the calculated intercalation energy, $E_{MnO_2/nLi}$ is the energy of the β-MnO_2 GB supercell with *n* intercalated Li ions, E_{MnO_2} is the energy of the β-MnO2 GB supercell, *n* is the number of Li ions, and E_{Li} is the energy of one Li ion in metallic bcc Li. The average equilibrium voltage, $\bar{V}$, is related to the difference in the Gibbs free energy, ΔG, between the delithiated phase (charged state) and lithiated phase (discharged state) by

$$\bar{V} = \frac{-\Delta G}{(n_2 - n_1)F} \quad (2)$$

where *F* is the Faraday constant. This calculation can be simplified by the fact that ΔG can be approximated by the internal (potential) energy change per intercalated Li^+ ion because the vibrational and configurational entropy contributions to the cell voltage at room temperature are expected to be small.

Li intercalation in β-MnO_2 occurs in a two-phase process upon first discharge to β-$LiMnO_2$ with a voltage of 3 V.[9,43] Previous GGA+U calculations[5] for bulk β-MnO_2 predicted a Li intercalation voltage of 3.2 V, in good agreement with experiment. In a similar study,[1] the average intercalation voltage corresponding to each Li intercalation stage was found to be 3.47 to 2.77 V, again in good agreement with the experiment voltage drop of 3.5 to 2.7 V.[11] The agreement between theory and experiment in these works is excellent considering that the computational studies only consider ideal cases and that entropic terms have been ignored. Furthermore, Ceder et al.[41,44] have reported typical underestimation errors of 0.5−0.7 V for the calculation of GGA intercalation voltages. As noted by Tompsett et al.,[5] these results also clearly show that the inability of bulk β-MnO_2 to intercalate Li is a result of kinetic barriers, not because it is thermodynamically unfavorable.

Figure 3 illustrates the four tunnel structures of the GB, each with one Li ion intercalated. In the 288 ion supercell, for each tunnel structure there are four potential doping sites, as shown for tunnel 1 in Figure 4. Therefore, for each unique tunnel structure, the maximum number of Li ions we can investigate

DOI: 10.1021/acsami.5b00775
ACS Appl. Mater. Interfaces 2015, 7, 8125−8131

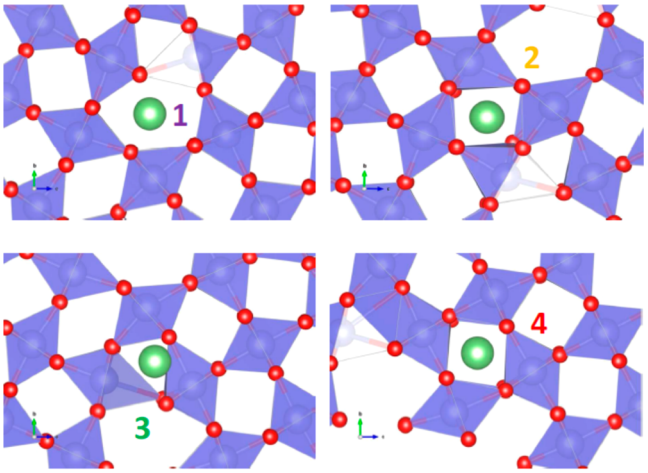

Figure 3. Optimized β-MnO2 Σ 5(210)/[001] GB tunnel structures each intercalated with one Li ion.

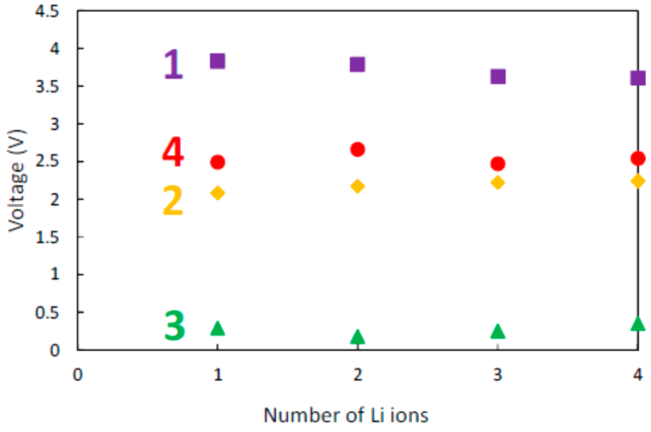

Figure 5. Intercalation voltage as a function of the number of Li ions for the four tunnel structures in the β-MnO_2 Σ 5(210)/[001] GB.

the intercalation voltage for is four. The DFT-GGA calculated Li intercalation voltages for the β-MnO_2 Σ 5(210)/[001] GB are plotted in Figure 4. Perhaps the most obvious feature of the intercalation voltages is that they differ dramatically depending on the tunnel structure. The largest voltages, 3.83−3.61 V, are observed for tunnel 1 and significantly larger than the values obtained for bulk β-MnO_2. This is to be expected given that this tunnel is the largest and therefore easiest for Li ions to locate. Furthermore, unlike for the other three tunnels, Li intercalation of tunnel 1 causes very little distortion to the surrounding structure, as shown by Figure 3. Tunnel 3 exhibits the lowest Li intercalation voltage, 0.29−0.35 V, as a result of the small, highly distorted tunnel structure. Tunnels 2 and 4 share similar intercalation voltages with tunnel 4, having the closest voltages, 2.49−2.54 V, to the bulk values.[9,22]

Our results suggest that while open GB structures will strongly promote Li intercalation, highly distorted, narrow structures may inhibit Li intercalation and also have a negative influence on the likelihood of Li intercalation at sites close or adjacent to the GB. We now consider Li migration properties at the β-MnO_2 Σ 5(210)/[001] GB (Figure 5).

3.3. GB Migration. The rate of diffusion of intercalated Li ions is a crucial parameter for battery materials as it determines the power output and battery charging times. While the intercalation voltage is also an essential property for battery materials, if the migration rate is poor, then the material is of no practical use. The Li migration properties of bulk β-MnO_2 have previously been studied.[1,5] As discussed previously, it has been proven experimentally and computationally that migration primarily occurs through the tunnel structures of the *c*-axis. Any other migration paths results in large distortions to the MnO_6 octahedra and are therefore energetically unfavorable.[5] Tompsett et al.[5] used GGA+U to calculate a value of 0.17 eV for Li migration in the bulk, while Wang et al.[1] obtained a value of 0.26 eV using the same functional. Both values suggest fast Li transport and intercalation kinetics and explain the excellent rate performance of mesoporous β-MnO_2. The difficulty of intercalating of Li into the bulk material has also been demonstrated by the high energy barrier of >0.6 eV for surface to bulk ion migration.[5]

The influence of Li ion migration at the GBs of β-MnO_2 has not yet been explored even though the importance of interfaces to both ionic and electronic conductivity in nanoionic battery materials has been previously highlighted.[42,43,44] The four Li migration pathways considered in this study are illustrated in Figure 6. We use the same four tunnel structures that were used for Li intercalation voltage calculations. Figure 7 shows the energy profiles for Li migration at the β-MnO_2 Σ 5(210)/[001] GB. Tunnel 1 has the lowest migration energy, 0.15 eV, and tunnel 3 the highest, 0.89 eV. The significant difference in

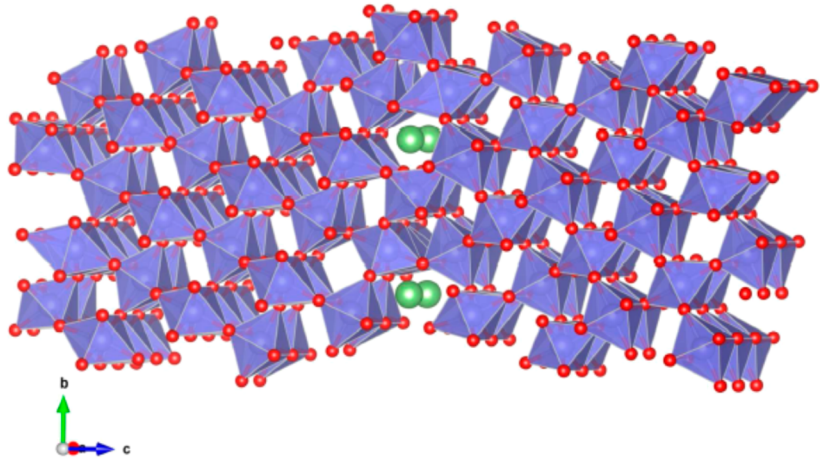

Figure 4. Optimized β-MnO_2 Σ 5(210)/[001] GB displaying the four doping sites for tunnel 1.

DOI: 10.1021/acsami.5b00775
ACS Appl. Mater. Interfaces 2015, 7, 8125−8131

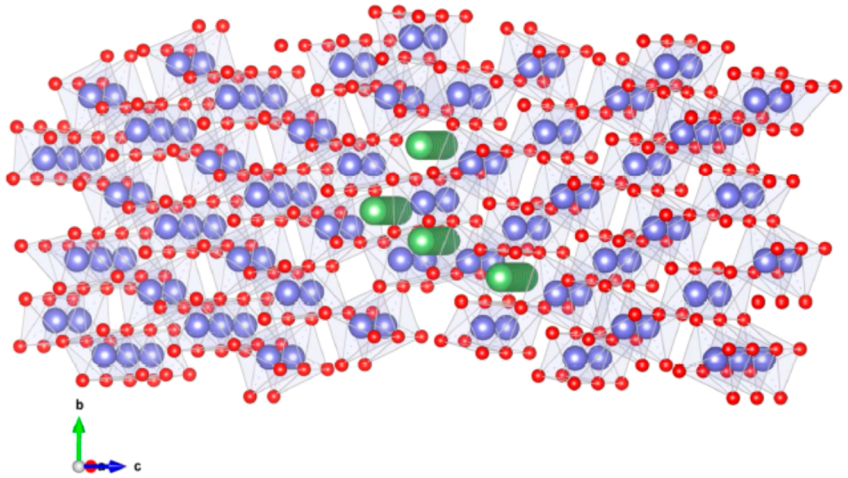

Figure 6. β-MnO_2 Σ 5(210)/[001] GB displaying the four migration paths considered in this work. The MnO_6 octahedra and Mn−O bonds have been made transparent for clarity.

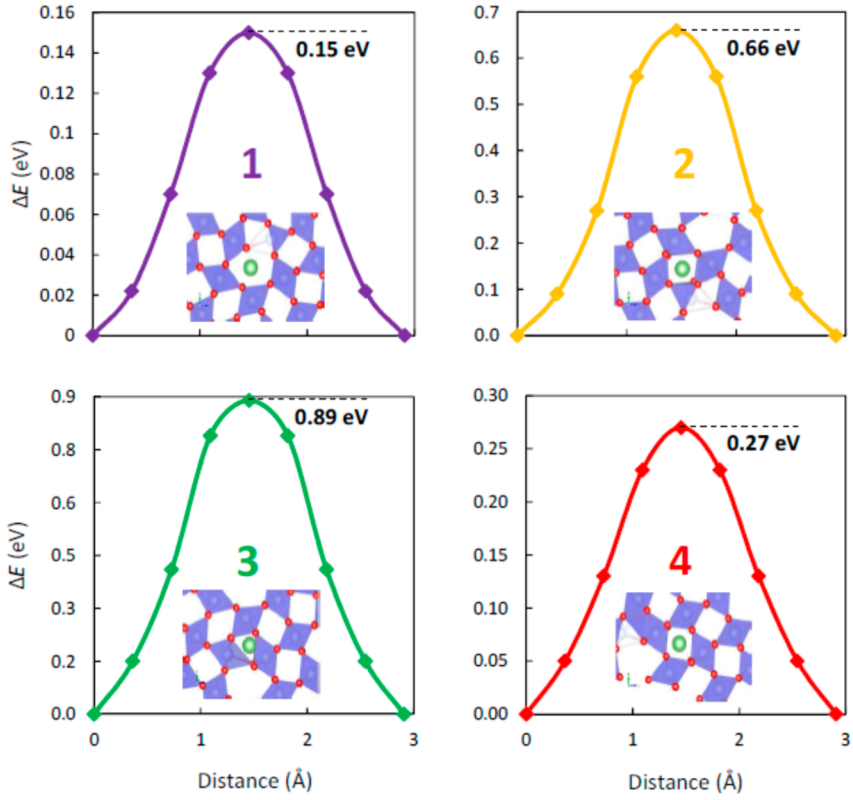

Figure 7. Energetics for Li migration through four of the unique tunnel structures of the β-MnO_2 Σ 5(210)/[001] GB.

energies for these two structures again highlights the same arguments made for Li intercalation, in that the wide ranging tunnel structures at the GB each have very unique electrochemical properties. Tunnel 2 also has a high migration energy of 0.66 eV, larger than even the value calculated for surface to bulk migration.[5] Tunnel 4, with the bulk-like structure, has a migration energy of 0.27 eV, somewhat higher than the values calculated for actual bulk β-MnO_2.[1,5]

As was the case for the intercalation voltages, it seems that local strain to the area surrounding the intercalated Li ion plays a large role in determining the properties. In fact, the migration energies follow the same order as for the intercalation voltages, in that the large open tunnel 1 has the best performance and the small, narrow tunnel 3 has the poorest performance. For tunnel 1, the migration energy is lower and the intercalation voltage is higher than that calculated of bulk β-MnO_2, which suggests fast transport and intercalation kinetics of Li through this structure and therefore, potentially, a higher specific capacity. Conversely, tunnel 3 displays both poor intercalation and a very high migration energy, rendering it useless for battery applications. Tunnels 2 and 4 both illustrate that even a small distortion, as a result of the GB, to the MnO_6 octahedra can result in a reduction in the electrochemical properties.

Overall, we have shown that open structures in β-MnO_2 GBs exhibit excellent electrochemical properties, while heavily distorted structures and even structures where the distortion

DOI: 10.1021/acsami.5b00775
ACS Appl. Mater. Interfaces 2015, 7, 8125−8131

is only slight exhibit inferior performance to the bulk material. As a result, it would seem that on the basis of our results, GBs play an important role in determining electrochemical performance. As the concentration of GBs is higher in nanostructured β-MnO_2 compared to the bulk and there are a sufficient number of open tunnels, this may help to explain the excellent performance of nanostructured samples. It must be noted that we have only considered one GB structure, albeit a very stable one, in this work because of the large computational expense, especially in calculating Li migration. To gain a full appreciation of the effect GBs have on these properties, other GBs must also be tested. We hope the procedure we have described in this work will be applied to many other battery and supercapacitor materials, as it likely to be an important factor for electrochemical performance.

4. CONCLUSIONS

Using GGA+U calculations, we have completed the first ever study of Li intercalation and migration at a β-MnO_2 GB. Building upon our previous work on the GBs of this important material, we used the low energy Σ 5(210)/[001] GB as a model to assess the effect GBs have on the electrochemical properties and performance as a cathode material.

Our calculations revealed that both the Li intercalation and transport properties are highly dependent on the local structures present at the GB and can vary dramatically as a result. It was shown that large tunnel structures in the GB can promote Li transport and intercalation with voltages of up to 3.83 eV, compared to the experimental value of 3.00 eV. Small tunnel structures, on the other hand, can hinder Li intercalation with significantly reduced voltages and high migration energies. On the basis of our results, GBs in β-MnO_2 have a strong influence on electrochemical performance and are a contributing factor to the excellent performance of nanostructured β-MnO_2, where the concentration of GBs is certainly higher than for bulk samples. However, if samples with narrow GB structures are engineered, then the GBs may actually become detrimental for electrochemical performance. The role of GBs in many battery materials is not yet fully understood or has been, so far, completely neglected. We hope the methods and results in the work will be applied to many different materials in the future so that a fuller understanding of the consequences of these interfaces can be achieved.

AUTHOR INFORMATION

Corresponding Author

*Phone: +81-75-753-5435. E-mail: doson5888@gmail.com.

Notes

The authors declare no competing financial interest.

ACKNOWLEDGMENTS

We thank the Japan Society for the Promotion of Science (JSPS) for funding through Grants-in-Aid for (a) Scientific Research on Innovative Areas "Nano Informatics" (grant no. 25106005) and for (b) JSPS fellows (grant no. 2503370).

REFERENCES

(1) Wang, D.; Liu, L.-M.; Zhao, S. J.; Li, B.-H.; Liu, H.; Lang, X.-F. β-MnO_2 as a Cathode Material for Lithium Ion Batteries from First Principles Calculations. *Phys. Chem. Chem. Phys.* **2013**, *15*, 9075.

(2) Armstrong, A. R.; Bruce, P. G. Synthesis of Layered $LiMnO_2$ as an Electrode for Rechargeable Lithium Batteries. *Nature* **1996**, *381*, 499−500.

(3) Armstrong, A. R.; Holzapfel, M.; Novak, P.; Johnson, C. S.; Kang, S.-H.; Thackeray, M. M.; Bruce, P. G. Demonstrating Oxygen Loss and Associated Structural Reorganization in the Lithium Battery Cathode $Li[Ni_{0.2}Li_{0.2}Mn_{0.6}]O_2$. *J. Am. Chem. Soc.* **2006**, *128*, 8694−8698.

(4) Tompsett, D. A.; Parker, S. C.; Islam, M. S. Rutile (β-)MnO_2 Surfaces and Vacancy Formation for High Electrochemical and Catalytic Performance. *J. Am. Chem. Soc.* **2014**, *136*, 1418−1426.

(5) Tompsett, D. A.; Parker, S. C.; Bruce, P. G.; Islam, M. S. Nanostructuring of β-MnO_2: The Important Role of Surface to Bulk Ion Migration. *Chem. Mater.* **2013**, *25*, 536−541.

(6) Cheng, F.; Zhang, T.; Zhang, Y.; Du, J.; Han, X.; Chen, J. Enhancing Electrocatalytic Oxygen Reduction on MnO_2 with Vacancies. *Angew. Chem., Int. Ed.* **2013**, *52*, 2474−2477.

(7) Dawson, J. A.; Tanaka, I. Oxygen Vacancy Formation and Reduction Properties of β-MnO_2 Grain Boundaries and the Potential for High Electrochemical Performance. *ACS Appl. Mater. Interfaces* **2014**, *6*, 17776−17784.

(8) Dawson, J. A.; Chen, H.; Tanaka, I. First-Principles Calculations of Oxygen Vacancy Formation and Metallic Behaviour at a β-MnO_2 Grain Boundaries. *ACS Appl. Mater. Interfaces* **2015**, *7*, 1726−1734 DOI: 10.1021/am507273c.

(9) Jiao, F.; Bruce, P. G. Mesoporous Crystalline β-MnO_2—A Reversible Positive Electrode for Rechargeable Lithium Batteries. *Adv. Mater.* **2007**, *19*, 657−660.

(10) Thackeray, M. M.; Johnson, C. S.; Vaughey, J. T.; Li, N.; Hackney, S. A. Advances in Manganese-Oxide 'Composite' Electrodes for Lithium-Ion Batteries. *J. Mater. Chem.* **2005**, *15*, 2257−2267.

(11) Luo, J.-Y.; Zhang, J.-J.; Xia, Y.-Y. Highly Electrochemical Reaction of Lithium in the Ordered Mesoporosus β-MnO_2. *Chem. Mater.* **2006**, *18*, 5618−5623.

(12) Cheng, F.; Zhao, J.; Song, W.; Li, C.; Ma, H.; Chen, J.; Shen, P. Facile Controlled Synthesis of MnO_2 Nanostructures of Novel Shapes and Their Application in Batteries. *Inorg. Chem.* **2006**, *45*, 2038−2044.

(13) Sayle, T. X. T.; Maphanga, R. R.; Ngoepe, P. E.; Sayle, D. C. Predicting the Electrochemical Properties of MnO_2 Nanomaterials Used in Rechargeable Li Batteries: Simulating Nanostructure at the Atomistic Level. *J. Am. Chem. Soc.* **2009**, *131*, 6161−6173.

(14) Bach, S.; Pereira-Ramos, J. P.; Willmann, P. A Kinetic Study of Electrochemical Lithium Insertion in Nanosized Rutile β-MnO_2 by Impedance Spectroscopy. *Electrochim. Acta* **2011**, *56*, 10016−10022.

(15) Kinoshita, K. *Electrochemical Oxygen Technology*, 1st ed; Wiley: New York, 1992.

(16) Wei, C.; Yu, L.; Cui, C.; Lin, J.; Wei, C.; Mathews, N.; Huo, F.; Sritharan, T.; Xua, Z. Ultrathin MnO_2 Nanoflakes as an Efficient Catalyst for Oxygen Reduction Reaction. *Chem. Commun.* **2014**, *50*, 7885−7888.

(17) Bruce, P. G.; Freunberger, S. A.; Hardwick, L. J.; Tarascon, J.-M. Li-O_2 and Li-S Batteries with High Energy Storage. *Nature Mater.* **2012**, *11*, 19−29.

(18) Devaraj, S.; Munichandraiah, N. Effect of Crystallographic Structure of MnO_2 on Its Electrochemical Capacitance Properties. *J. Phys. Chem. C* **2008**, *112*, 4406−4417.

(19) Zang, J.; Li, X. In situ Synthesis of Ultrafine β-MnO_2/Polypyrrole Nanorod Composites for High-Performance Supercapacitors. *J. Mater. Chem.* **2011**, *21*, 10965−10969.

(20) Mellan, T. A.; Maenetja, K. P.; Ngoepe, P. E.; Woodley, S. M.; Catlow, C. R. A.; Grau- Crespo, R. Lithium and Oxygen Adsorption at the β-MnO_2 (110) Surface. *J. Mater. Chem., A* **2013**, *1*, 14879−14887.

(21) Oxford, G. A. E.; Chaka, A. M. First-Principles Calculations of Clean, Oxidized, and Reduced β-MnO_2 Surfaces. *J. Phys. Chem. C* **2011**, *115*, 16992−17008.

(22) Oxford, G. A. E.; Chaka, A. M. Structure and Stability of Hydrated β-MnO_2 Surfaces. *J. Phys. Chem. C* **2012**, *116*, 11589−11605.

(23) Li, L.; Wei, Z.; Chen, S.; Qi, X.; Ding, W.; Xia, M.; Li, R.; Xiong, K.; Deng, Z.; Gao, Y. A Comparative DFT Study of the Catalytic Activity of MnO_2 (211) and (2-2-1) Surfaces for an Oxygen Reduction Reaction. *Chem. Phys. Lett.* **2012**, *539*, 89−93.

DOI: 10.1021/acsami.5b00775
ACS Appl. Mater. Interfaces 2015, 7, 8125−8131

(24) Perdew, J. P.; Burke, K.; Ernzerhof, M. Generalized Gradient Approximation Made Simple. *Phys. Rev. Lett.* **1996**, *77*, 3865.
(25) Blochl, P. E. Projector Augmented-Wave Method. *Phys. Rev. B* **1994**, *50*, 17953.
(26) Kresse, G.; Furthmuller, J. Efficiency of ab Initio Total Energy Calculations for Metals and Semiconductors Using a Plane-Wave Basis Set. *Comput. Mater. Sci.* **1996**, *6*, 15−50.
(27) Schwarz, K.; Blaha, P. Solid State Calculations using WIEN2k. *Comput. Mater. Sci.* **2003**, *28*, 259−273.
(28) Madsen, G. K. H.; Novak, P. Charge Order in Magnetite. An LDA+U Study. *Europhys. Lett.* **2005**, *69*, 777−783.
(29) Tompsett, D. A.; Middlemiss, D. S.; Islam, M. S. Importance of Anisotropic Coulomb Interactions and Exchange to the Band Gap and Antiferromagnetism of β-MnO_2 from DFT+U. *Phys. Rev. B* **2012**, *86*, 205126.
(30) Chabre, Y.; Pannetier, J. Structural and Electrochemical Properties of the Proton/γ-MnO_2 System. *Prog. Solid State Chem.* **1995**, *23*, 1.
(31) MacLean, L. A. H.; Tye, F. L. The Structure of Fully H-Inserted γ-Manganese Dioxide Compounds. *J. Solid State Chem.* **1996**, *123*, 150.
(32) Dias, D.; Carvalho, P. A.; Ferro, A. C.; Lohwasser, W. MnO_2 Counter-Electrode Structure in Ta Capacitors: A TEM Study. *Acta Mater.* **2005**, *53*, 4723.
(33) Maphanga, R. R.; Sayle, D. C.; Sayle, T. X. T.; Ngoepe, P. E. Amorphization and Recrystallization Study of Lithium Insertion into Manganese Oxide. *Phys. Chem. Chem. Phys.* **2010**, *13*, 1307.
(34) Korner, W.; Elsasser, C. Density Functional Theory Study of Dopants in Polycrystalline TiO_2. *Phys. Rev. B* **2011**, *83*, 205315.
(35) Dawson, I.; Bristowe, P. D.; Lee, M. H.; Payne, M. C.; Segall, M. D.; White, J. A. First-Principles Study of a Tilt Grain Boundary in Rutile. *Phys. Rev. B* **1996**, *54*, 13727−13733.
(36) Sinnott, S. B.; Wood, R. F.; Pennycook, S. J. Ab Initio Calculations of Rigid-Body Displacements at the Σ5 (210) Tilt Grain Boundary in TiO_2. *Phys. Rev. B* **2000**, *61*, 15645−15648.
(37) Baur, W. Rutile-Type Compounds. V. Refinement of MnO_2 and MgF_2. *Acta Crystallogr., Sect. B: Struct. Sci.* **1976**, *32*, 2200−2204.
(38) Ren, Y. *Applications of Ordered Mesoporous Metal Oxides: Energy Storage, Adsorption, and Catalysis*. Ph.D. Thesis. University of St. Andrews, 2010.
(39) Thackeray, M. M. Manganese Oxides for Lithium Batteries. *Prog. Solid State Chem.* **1997**, *25*, 1−71.
(40) David, W. I. F.; Thackeray, M. M.; Bruce, P. G.; Goodenough, J. B. Lithium Insertion into β-MnO_2 and the Rutile-Spinel Transformation. *Mater. Res. Bull.* **1984**, *19*, 99−106.
(41) Ceder, G.; Hautier, G.; Jain, A.; Ong, S. P. Recharging Lithium Battery Research with First-Principles Methods. *MRS Bull.* **2011**, *36*, 185−191.
(42) Islam, M. S.; Fisher, C. A. J. Lithium and Sodium Battery Cathode Materials: Computational Insights into Voltage, Diffusion and Nanostructural Properties. *Chem. Soc. Rev.* **2014**, *43*, 185−204.
(43) Ren, Y.; Armstrong, A. R.; Jiao, F.; Bruce, P. G. Influence of Size on the Rate of Mesoporous Electrodes for Lithium Batteries. *J. Am. Chem. Soc.* **2010**, *132*, 996−1004.
(44) Ceder, G. Opportunities and Challenges for First-Principles Materials Design and Applications to Li Battery Materials. *MRS Bull.* **2010**, *35*, 693−701.

DOI: 10.1021/acsami.5b00775
ACS Appl. Mater. Interfaces 2015, 7, 8125−8131